Published in final edited form as:

Carbon N Y. 2013 November ; 64: 341–350. doi:10.1016/j.carbon.2013.07.084.

Luminescent graphene quantum dots fabricated by pulsed laser synthesis

Khaled Habiba[a,b,*], **Vladimir I. Makarov**[a,b], **Javier Avalos**[a,c], **Maxime J.F. Guinel**[a,b,d], **Brad R. Weiner**[a,d], and **Gerardo Morell**[a,b]

[a]Institute of Functional Nanomaterials, University of Puerto Rico, San Juan, PR 00931-3334, USA

[b]Department of Physics, University of Puerto Rico – Rio Piedras Campus, San Juan, PR 00936-8377, USA

[c]Department of Physics, University of Puerto Rico – Bayamon Campus, Bayamon, PR 00959, USA

[d]Department of Chemistry, University of Puerto Rico – Rio Piedras Campus, San Juan, PR 00931-3346, USA

Abstract

Graphene has been the subject of intense research in recent years due to its unique electrical, optical and mechanical properties. Furthermore, it is expected that quantum dots of graphene would make their way into devices due to their structure and composition which unify graphene and quantum dots properties. Graphene quantum dots (GQDs) are planar nano flakes with a few atomic layers thick and with a higher surface-to-volume ratio than spherical carbon dots (CDs) of the same size. We have developed a pulsed laser synthesis (PLS) method for the synthesis of GQDs that are soluble in water, measure 2–6 nm across, and are about 1–3 layers thick. They show strong intrinsic fluorescence in the visible region. The source of fluorescence can be attributed to various factors, such as: quantum confinement, zigzag edge structure, and surface defects. Confocal microscopy images of bacteria exposed to GQDs show their suitability as biomarkers and nano-probes in high contrast bioimaging.

1. Introduction

Graphene is a unique material that has attracted many researchers due to its chemical stability, and good optical, thermal, electronic and mechanical properties. These properties make graphene and graphene derivatives excellent materials for various applications [1–4]. There are many reports on the properties and applications of various types of carbon nanostructures, some based on theoretical analysis [5–7], and others on experimental data, such as the synthesis of graphene quantum dots GQDs [8–23], and carbon dots [24– 31].

[*]*Corresponding author*. Address: Institute for Functional Nanomaterials, University of Puerto Rico, Rio Piedras Campus, San Juan, PR 00931, USA. Fax: +1 787 764 4063. khabiba@gmail.com, khaled.habiba@upr.edu (K. Habiba).

Appendix A. Supplementary data

Supplementary data associated with this article can be found, in the online version, at http://dx.doi.org/10.1016/j.carbon.2013.07.084.

According to these reports, the properties of carbon nano-structures depend, in general, on their size, shape, and surface chemical composition.

Graphene quantum dots are relatives to carbon dots but they are different in structure and properties [16,17,24]. Specifically, carbon dots are spherical nanocrystals of graphite with high concentration of oxygen due to their surface oxidation, and their average size distribution is less than 10 nm [16,17,24–31]. In comparison, GQDs are planar nanocrystals of graphene with higher surface-to-volume ratio and with size distribution in the range of 2–20 nm across [8–23]. The higher surface-to-volume ratio of GQDs provides a better driving force for diffusion, which is important in biomedical applications. Moreover, GQDs can have intrinsic luminescence due to quantum confinement, surface defects, and edge structure, unlike carbon dots, which fluoresce only from their surface defects caused by oxidation [24].

Although the optical properties of monolayer graphene are very attractive, its optoelectronic properties are poor due to its zero bandgap [2,9,32]. Gokus et al. [33] showed photoluminescence in graphene after oxygen plasma treatment, probably due to electron confinement of sp^2 islands of 1 nm average size. Quantum confinement effects can be observed in graphene nanostructures of less than 20 nm, such as graphene nano ribbons and graphene quantum dots [8,18]. However, for carbon dots, the quantum effect was observed only for particles of less than 10 nm, which makes graphene quantum dots more attractive [16,24].

GQDs are similar to inorganic quantum dots (*i.e.*, CdSe, PbS, ZnS and GaN) in their optoelectronic properties. They are nevertheless ecofriendly and essentially nontoxic, unlike inorganic quantum dots which have shown high cytotoxicity [34]. However, GQDs photoluminescence (PL) is not only dependent on size, but on other parameters that depend on the synthesis method, such as defects and surface oxidation, that can change their PL properties [8–23].

Many different techniques have been reported for the synthesis of GQDs, including nanolithography [8], top-down synthesis [12,14–16,20], and bottom-up synthesis [10,11,18]. GQDs have also been produced starting from a commercial material, such as in the chemical oxidation and cutting of carbon fibers [9], or by exfoliation of carbon nanotubes [13]. Almost all of these techniques are, in general, relatively complex and expensive. Herein, we report a new method for the synthesis of intrinsically luminescent GQDs by liquid phase PLS.

2. Experimental

2.1. Synthesis of GQDs

A mixture of 0.255 wt.% nickel (II) oxide powder (Alfa Aesar, green) in 99.745 wt.% benzene (Sigma Aldrich, anhydrous 99.8%) was irradiated for 30 min with a 1064 nm pulsed Nd:Yag laser (Continuum Surelite, 10 Hz, 10 ns pulse width). The laser power density was adjusted to 15.9×10^8 W cm^{-2}, corresponding to laser energy of about 30 mJ/pulse. The mixture of GQDs, NiO and benzene was centrifuged at 5000 rpm for 15 min,

leaving the GQDs in the supernatant, while the NiO particles remained in the pellet. The GQDs were then separated from the benzene by rotor evaporation, and dissolved in deionized water. The water solution of the GQDs was centrifuged at 10,000 rpm, and finally, filtered using syringe filters (Millipore, 0.05 μm pore size). The pH of the final GQDs solution was adjusted to 7.4. The yield of the synthesized GQDs obtained is about 100–200 mg.

2.2. Characterizations

High resolution transmission electron microscopy (HR-TEM) and electron energy loss spectroscopy (EELS) data were recorded using a JEOL JEM-2200FS TEM operated at 200 kV. Raman spectroscopy was carried on using a Horiba Jobin-Yoon T-6400 Raman microprobe and a diode Laser with a wavelength of 532 nm. The Fourier transform infrared (FT-IR) spectrum was obtained using a Bruker Tensor 27 using ATR-FT-IR technique. AFM measurements were performed in tapping mode using a Veeco Nanoscope III. XPS experiments were performed with the Physical Electronics 1257, Al K_{α} source, 200 mm diameter analyzer. ^{1}H NMR spectra were recorded on a Bruker Advance AV-500 (500 MHz), the sample was dissolved in deuterated benzene. The UV–Visible spectra were recorded on a Varian Cary 1E UV spectrophotometer. For PL characterizations, the excitation and emission spectra of the GQDs solutions were recorded using a Varian Cary Eclipse (Xenon lamp as an excitation source). The confocal microscope images were recorded using a Zeiss observer Z-1 and laser LSM 510 META, the images were recorded on a magnification of 100× and the excitation wavelengths used were 405 nm, 488 nm, and 561 nm.

2.3. Preparation of bacterial cells for imaging

Pseudomonas aeruginosa bacteria pellets were commercially acquired (0353E3, MicroBiologics, MN, USA). The initial concentration of bacteria strain was of 4.9×10^{3} colony-forming units (CFUs)/mL diluted in 20 mL of nutrient broth and incubated at 35 °C during 48 h. Two bacterial population growth curves were obtained one for control (bacteria without GQDs) and one for bacteria incubated with GQDs. The control curve was obtained by adding 10 mL of the inoculated *P. aeruginosa* into 40 mL of nutrient broth. The bacteria-GQDs growth curve was obtained by adding 10 mL of the inoculated *P. aeruginosa* into 38 mL of nutrient broth and 2 mL of GQDs (12.6 mg/mL). Both the control and bacteria with GQDs were incubated at 37 °C for 3 h at 110 rpm. The absorbance for both the control and the incubated GQDs with bacteria were monitored and recorded using a UV–Visible spectrophotometer (Helios, 640 nm), until reaching the middle of the log phase in the bacterial population growth curve. Then 2 mL of bacteria incubated with GQDs were centrifuged at 10,000 rpm for 10 min to separate the bacteria pellet from the nutrient broth and the GQDs localized outside the membrane of the bacteria. The incubated bacteria with GQDs were washed three times by phosphate buffer (PBS) with pH = 7.4, and then finally the pellet was suspended in 1 mL of PBS using a vortex. For con-focal microscopy imaging, a few drops of the bacterial cells were placed in a chamber covered glass cell (Thermo Scientific, Nunc Lab-Tek II) and different excitation wavelengths (*i.e.*, 405 nm, 488 nm, and 561 nm) were employed. The same procedures for microscope cell preparation and the same parameters for confocal microscopy imaging were employed for the control bacteria.

3. Results and discussion

We prepared carbon nanoparticles in liquid phase by pulsed laser synthesis (PLS). The method consists of a suspension of nickel oxide (as catalyst) in benzene (carbon source) that is laser irradiated, as described in Fig. 1. Before performing the physical and chemical characterizations, it was unknown if the nanoparticles were GQDs, CDs or something else.

The carbon nanoparticles were dissolved in DI water, methanol and ethanol to a concentration of 24 mg/mL. The solutions look weak pale yellow in visible light. When they are subjected to UV light (excitation wavelength 254 nm), blue fluorescence is readily seen to the naked eye, as shown in Fig. 2. The different colors noted in the fluorescence of the particles in these solvents are most likely due to solvent attachment or different emissive traps on the surface of GQDs [14]. The PL emission spectra of GQDs in water, ethanol and methanol at the same excitation wavelength (254 nm) are shown in Fig. S1 (see Supplementary information). The spectra have distinct emission peaks in methanol, show broadening in ethanol, and the features are no longer evident in water. One possibility is that this behavior is due to hydrogen bonding between the GQDs and the solvent, resulting from increasing polarizability of the solvent O–H bond from methanol to ethanol to water.

We set out to find specific information about the luminescent carbon nanoparticles to determine if they are GQDs, carbon dots, or other types of carbon nanostructures. High resolution transmission electron microscope (HR-TEM) shows that the size of the carbon nanoparticles is in range of 2–6 nm, as illustrated in Fig. 3a. Statistical analyses of the HR-TEM images gives a Gaussian distribution as shown in Fig. 3b of particle sizes centered at 3.42 nm with a full width at half maximum (FWHM) of 1.32 nm, which represents a narrow size distribution. Fig. 3c clearly shows the crystalline structure of the nanoparticles. The measured lattice spacing is 0.213 nm, corresponding to the {1100} lattice fringes of graphene [22,35]. Fig. 3d shows a graphene nanoparticle under high resolution and the corresponding Fast fourier transformation (FFT) in the inset. The indexation is consistent with the structure of graphene [21,35,36]. The schematic in Fig. 3e shows the hexagonal structure of graphene compared to the same image shown in Fig. 3d. The edges are parallel to the zigzag direction, as in graphene synthesized by other methods [9,12,13]. The distance between the carbon–carbon bonds in the hexagonal structure is between 0.136 and 0.144 nm (average distance is 0.140 nm), in agreement with numerical values of GQDs [19], and close to experimental values of GQDs (*i.e.*, 0.142–0.144 nm) [12,13]. The accuracy of the measurements is ±5%.

Electron energy loss spectroscopy (EELS) was employed to investigate the chemical composition of the synthesized nanoparticles. EELS measurements shown in Fig. 4 are dominated by the carbon edge region that shows 1s–π^* transition of sp^2 bonded carbon at 285 eV, and the 1s–σ^* transition of sp^3 bonded carbon at 292 eV, consistent with EELS of GQDs synthesized by other methods [10,12]. A weak signal of the oxygen K-edge at 539 eV is also present, as expected for water-soluble GQDs [10].

Taken altogether, the above-described analyses indicate that the fluorescent carbon nanoparticles fabricated by PLS (bottom-up approach) are indistinguishable from GQDs

synthesized by hydrothermal cutting of graphene sheets (top-down approach) [12,15,16,20]. Hence, from this point forward we refer to these carbon nanoparticles as GQDs. Moreover, in comparison with the microwave-assisted hydrothermal bottom-up method [10] that requires energies in the range from 30 to 300 kJ, the PLS bottom-up method hereby described requires only 600–700 J of applied laser power to yield 100–200 mg of net GQDs.

The GQDs were also imaged using AFM in contact mode to investigate their average height and determine the average number of graphene layers, as shown in Fig. 5. The GQDs were placed on a mica substrate and many selected lines were taken on different places on the substrate on different particles (see Fig. 5a). The histogram shows that particles height distribution is between 0.4 and 3.2 nm (see Fig. 5b). The highest fraction of GQDs has a height of 1.5 nm. This height corresponds to about 2 graphene layers, which is in agreement with GQDs synthesized by other methods [9,14]. Note that the height of spherical carbon dots is 4–7 nm, much higher than that of GQDs [27].

The Raman spectrum in Fig. 6 shows the D-band at 1352 cm^{-1} arising from the disorder in sp^2 hybridized carbon, and the G-band at 1594 cm^{-1} corresponding to graphitic structures. The G-band is shifted from 1581 cm^{-1} in graphite to 1594 cm^{-1} in nano-crystalline graphite, due to the merging of the D′ and G bands [37]. The broad bands centered at 2670 cm^{-1} and 2929 cm^{-1} correspond to the 2D and D + G bands, respectively [38]. They arise from the relaxation in selection rules caused by phonon scattering at boundaries and defects in GQDs [37,39,40]. The ratio of intensities of D band with respect to G band, I(D)/I(G), is around 0.93, which is related to the crystal size. As reported by Tuinstra and Koenig [41], I(D)/I(G) varies inversely with the cluster size L_a in nanocrystalline graphite according to this relationship: $I(D)/I(G) = C(\lambda)/L_a$, where $C(\lambda)$ is an empirical constant that depends on the excitation laser energy and C (λ = 515.5 nm) = 4.4 nm [33,41,42]. According to this relation, the average size of the GQDs is L_a = 4.7 nm, which falls within the 2–6 nm range obtained by HR-TEM data described above.

In order to investigate the presence of functional groups attached to the surface of the GQDs, we employed Fourier transform infrared spectroscopy (FT-IR) and X-ray photoelectron spectroscopy (XPS).

The FT-IR spectrum of the GQDs in Fig. 7 reveals the presence of C–O groups at 1020 cm^{-1}, and hydroxyl groups at 3327 cm^{-1} (O–H stretching) [10]. These groups are responsible for the solubility of the GQDs in water [9]. The absorptions observed at 2930 cm^{-1} and 1380 cm^{-1} correspond to C–H, which is also present on the surface of GQDs. The absorption observed at 1620 cm^{-1} is attributed to the presence of the aromatic rings C=C, while absorption peak at 830 cm^{-1} is attributed to the aromatic CH_2 rocking, as observed in GQDs synthesized by the microwave-assisted hydrothermal method [10].

The XPS survey spectrum of the GQDs after separation from the nickel oxide is shown in Fig. S2 (see Supplementary information). A few drops of GQDs solution were placed on the surface of a silicon oxide substrate and dried for XPS characterization, which explains the presence of the Si lines in the spectrum. There is no sign of presence of Ni, which would have been found in the 850–890 eV region. The XPS high resolution spectrum in Fig. 8

shows the C1s carbon. The deconvoluted spectrum shows four bands at 284.6 eV, 286.3 eV, 287.85 eV, and 289.58 eV corresponding to sp^2 aromatic carbon, −C−OH (hydroxyl), −C−O −C− (ether), and O=C–OH (car-boxyl), respectively. They are in agreement with the FT-IR results. These functional groups enable the solubility of GQDs in water, as is the case in GQDs synthesized by other methods [9,10]. The importance of the functional groups on the surface of the GQDs is not limited to solubility in water but, in addition, they generate surface states that act as charge traps and induce luminescence [9,29].

Complementing the XPS data, we show the ^{1}H Nuclear Magnetic Resonance Spectrum (NMR) in Fig. S3. It contains signals in the aromatic proton resonance region (7–8 ppm) that are consistent with the presence of aromatic condensed ring systems, as in GQDs, and with the structure of the GQDs shown in HR-TEM images.

After characterizing the chemical composition and structure of the synthesized GQDs, we construe that the irradiation of organic liquids generates suitable conditions locally for the formation of graphene moieties with certain number of conjugated carbon atoms,[1] similar to the ones obtained by other bottom-up methods [11,18].

One possible mechanism is that when the pulsed laser beam is focused inside the mixture of benzene and catalyst, it creates short lived plasma of a few 1000 K. In addition, there may be cavitation effect caused by the strong acoustic wave induced by laser pulses in liquid media. Together, the short lived plasma and cavitation effect create the conditions that lead to the synthesis of GQDs in the mixture of benzene and catalyst. Due to the fact that the fraction of aromatic ring clusters is critical for tuning the PL emission of graphene [2,9,32,33], benzene is an excellent medium for the synthesis of GQDs.

To investigate the optical properties of the GQDs, we employed UV–Visible spectroscopy, photoluminescence excitation (PLE), and PL emission. The UV–Visible absorption spectrum in Fig. 9 corresponds to the synthesized GQDs dissolved in water. It showed absorption bands around (a) 217 nm, (b) 267 nm, and (c) 335 nm, which are close to those of GQDs synthesized by exfoliation of carbon nanotubes and graphite flakes (*i.e.*, 207 nm, 260 nm, and 310 nm) [13]. The band at 217 nm is assigned to the transition between the π–π^* orbitals similarly to the absorption band in graphene oxide ~200 nm [32]. The bands at 267 nm and 335 nm most likely arise from oxygen related surface states, and correspond to the n–π^* transition of the C=O bond [13].

The PL emission of the GQDs shifts from 450 nm to 540 nm as the excitation wavelength changes from 350 nm to 460 nm (see Fig. 10). The maximum PL emission intensity occurred at 450 nm when it was excited at 350 nm with a Stokes shift of 100 nm. A similar dependence of PL emission on excitation wavelength has been reported for GQDs synthesized by various methods [8–23]. Also shown in Fig. 10 is the PLE spectrum recorded at the highest emission wavelength observed (λ = 450 nm). It consists of one peak at (a) 237 nm (5.23 eV), and two shoulders at (b) 285 nm (4.35 eV) and (c) 334 nm (3.71 eV). The highest energy peak is assigned to an absorption band corresponding to the π–π^* transition.

[1]Unpublished results from our laboratory.

Triplet carbenes have two orbitals (σ and π) which are singly occupied and commonly exist at the zigzag edges of the graphene [15]. The carbene ground state multiplicity requires that δE between σ and π orbitals be less than 1.5 eV for a triplet ground state, as reported by Hoffman [43]. Since the calculated δE is 0.64 eV and less than the 1.5 eV, hence, the two transitions represented in bands (b) and (c) in the PLE spectrum can be assigned to triplet carbene at the zigzag edges of graphene. This can also explain the source of the blue photoluminescence of GQDs as coming from the irradiation decay of activated electrons from the LUMO to the HOMO in these zigzag emissive sites [9,15].

In addition, the PL intensity varies with the pH of the solution (see Fig. 11) becoming stronger at higher pH values. The intensity observed at a pH of 10 is almost twice compared to a pH of 3.2. This effect can be ascribed to the protonation of the free zigzag sites by the acidic medium and the formation of complexes between the H^+ and the zigzag sites [9,44]. This assignment also explains the drop in the PL intensity of GQDs in acidic medium and is consistent with the above interpretation that the zigzag emissive sites are a source of PL emission.

The preliminary measurement of PL quantum yield of GQDs gives 0.055 at pH = 7.4, using anthracene in ethanol as a reference (known quantum yield = 0.3). This value is high compared to GQDs synthesized by oxidation of graphite (*i.e.* 0.01–0.03) [23], and low compared to other reported GQDs (*i.e.* 0.07–0.11) [10,14,17]. These authors have reported that the measurement of the PL quantum yield is still challenging in GQDs, as the surface passivation of GQDs by polyethylene glycol or by some ligands can increase the PL quantum yield of GQDs significantly. As we mentioned, the pH has a crucial effect on the PL emission of the particles. The measurement of the PL quantum yield is expected to give higher values in alkaline medium, and depends upon the passivation of the surface [10,17]. The calculation of the PL quantum yield of GQDs is added to the Supplementary information S4.

The PL properties of GQDs and their biocompatibility make them strong candidates for nano-probes in living cells [9,14,23]. In this context, we tested their suitability for confocal microscopy applications by imaging *P. aeruginosa* bacteria incubated in a medium containing GQDs. We added 2 mL of GQDs (12 mg/mL) to 10 mL of bacteria and 38 mL of nutrient broth. The bacteria were then incubated for 3 h. Fig. 12a – d show the confocal microscope images of the bacterial cells incubated with our synthesized GQDs. It is readily seen that the bacteria have a strong affinity for the GQDs, thus enhancing their imageability under the confocal microscope at 405, 488 and 561 nm excitation wavelengths. The merged image shown in Fig. 12e shows the high contrast images of the labeled bacteria. No signs of photobleaching were observed at all during 1 h of continuous irradiation. The self-luminescence of these bacteria is much weaker in comparison, as shown in Fig. 12f. Therefore, the GQDs hereby synthesized by PLS can be used as a high contrast probes in bio-imaging and in other applications, such as bacterial cell tracking and labeling of different types of bacteria for in situ studies. The GQDs are reportedly non-toxic [9,14,23], which render them suitable for other biological applications, such as biomolecules analysis by Fluorescence resonance energy transfer (FRET) and cancer cell imaging.

4. Summary

A novel method was demonstrated for the synthesis of water soluble GQDs by using PLS from benzene. The synthesized GQDs have strong luminescence in the visible region that makes them attractive for numerous biological applications. The luminescence arises from various sources, including quantum confinement, surface defects, and edge shape. The as-synthesized GQDs are very small, soluble in water, and they have high surface-to-volume ratio which provides to them excellent driving force in diffusion. These properties make them attractive in biomedical applications like nanoprobes for confocal microscope. Furthermore, by controlling the GQDs size distribution it should be possible to tune their PL emission for various applications, such as photovoltaic cells.

Supplementary Material

Refer to Web version on PubMed Central for supplementary material.

Acknowledgments

This research was carried out under the auspices of the Institute for Functional Nanomaterials (NSF Cooperative Agreement 1002410), PR NASA EPSCoR (NASA Cooperative Agreement NNX13AB22A) and PR DOE EPSCoR (DOE Grant DE-FG02-08ER46526). We want to acknowledge Dr. R. Arce for training and access to the Photochemistry Lab; Dr. E. Mosquera from University of Chile for providing XPS characterizations; J.A. Hernandez and Dr. L. Fonseca for their assistance in AFM imaging; J.R. Martinez and Dr. J.A. Prieto for providing the NMR facility; O. Medina and R. Velazquez for the bacteria culture; B. Madera and Dr. J. Lasalde for the confocal microscopy images.

REFERENCES

1. Geim AK, Novoselov KS. The rise of graphene. Nat Mater. 2007; 6(3):183–191. [PubMed: 17330084]
2. Eda G, Chhowalla M. Chemically derived graphene oxide: towards large-area thin-film electronics and optoelectronics. Adv Mater. 2010; 22(22):2392–2415. [PubMed: 20432408]
3. Loh KP, Bao Q, Ang PK, Yang J. The chemistry of graphene. J Mater Chem. 2010; 20(12):2277–2289.
4. Li D, Muller MB, Gilje S, Kaner RB, Wallace GG. Processable aqueous dispersions of graphene nanosheets. Nat Nanotechnol. 2008; 3(2):101–105. [PubMed: 18654470]
5. Wimmer M, Akhmerov AR, Guinea F. Robustness of edge states in graphene quantum dots. Phys Rev B. 2010; 82(4):045409.
6. Son YW, Cohen ML, Louie SG. Energy gaps in graphene nanoribbons. Phys Rev Lett. 2006; 97(21):216803. [PubMed: 17155765]
7. Barone V, Hod O, Scuseria GE. Electronic structure and stability of semiconducting graphene nanoribbons. Nano Lett. 2006; 6(12):2748–2754. [PubMed: 17163699]
8. Ponomarenko LA, Schedin F, Katsnelson MI, Yang R, Hill EW, Novoselov KS, et al. Chaotic dirac billiard in graphene quantum dots. Science. 2008; 320(5874):356–358. [PubMed: 18420930]
9. Peng J, Gao W, Gupta BK, Liu Z, Romero-Aburto R, Ge L, et al. Graphene quantum dots derived from carbon fibers. Nano Lett. 2012; 12(2):844–849. [PubMed: 22216895]
10. Tang L, Ji R, Cao X, Lin J, Jiang H, Li X, et al. Deep ultraviolet photoluminescence of water-soluble self-passivated graphene quantum dots. ACS Nano. 2012; 6(6):5102–5110. [PubMed: 22559247]
11. Liu R, Wu D, Feng X, Mu¨llen K. Bottom-up fabrication of photoluminescent graphene quantum dots with uniform morphology. J Am Chem Soc. 2011; 133(39):15221–15223. [PubMed: 21894989]

12. Kim S, Hwang SW, Kim MK, Shin DY, Shin DH, Kim CO, et al. Anomalous behaviors of visible luminescence from graphene quantum dots: interplay between size and shape. ACS Nano. 2012; 6(9):8203–8208. [PubMed: 22881035]
13. Lin L, Zhang S. Creating high yield water soluble luminescent graphene quantum dots via exfoliating and disintegrating carbon nanotubes and graphite flakes. Chem Commun. 2012; 48(82):10177–10179.
14. Zhu S, Zhang J, Qiao C, Tang S, Li Y, Yuan W, et al. Strongly green-photoluminescent graphene quantum dots for bioimaging applications. Chem Commun. 2011; 47(24):6858–6860.
15. Pan D, Zhang J, Li Z, Wu M. Hydrothermal route for cutting graphene sheets into blue-luminescent graphene quantum dots. Adv Mater. 2010; 22(6):734–738. [PubMed: 20217780]
16. Shen J, Zhu Y, Yang X, Zong J, Zhang J, Li C. One-pot hydrothermal synthesis of graphene quantum dots surface-passivated by polyethylene glycol and their photoelectric conversion under near-infrared light. New J Chem. 2012; 36(1):97–101.
17. Shen J, Zhu Y, Yang X, Li C. Graphene quantum dots: emergent nanolights for bioimaging, sensors, catalysis and photovoltaic devices. Chem Commun. 2012; 48(31):3686–3699.
18. Li LS, Yan X. Colloidal graphene quantum dots. J Phys Chem Lett. 2010; 1(17):2572–2576.
19. Philpott MR, Kawazoe Y. Graphene nanodots with intrinsically magnetic protrusions. J Chem Phys. 2012; 136(6):064706. [PubMed: 22360214]
20. Pan D, Guo L, Zhang J, Xi LC, Xue Q, Huang H, et al. Cutting sp^2 clusters in graphene sheets into colloidal graphene quantum dots with strong green fluorescence. J Mater Chem. 2012; 22(8): 3314–3318.
21. Shang NG, Papakonstantinou P, Sharma S, Lubarsky G, Li M, McNeill DW, et al. Controllable selective exfoliation of high-quality graphene nanosheets and nanodots by ionic liquid assisted grinding. Chem Commun. 2012; 48(13):1877–1879.
22. Lee J, Kim K, Park WI, Kim BH, Park JH, Kim TH, et al. Uniform graphene quantum dots patterned from self-assembled silica nanodots. Nano Lett. 2012; 12(12):6078–6083. [PubMed: 23148730]
23. Sun Y, Wang S, Li C, Luo P, Tao L, Weia Y, et al. Large scale preparation of graphene quantum dots from graphite with tunable fluorescence properties. Phys Chem Phys. 2013; 15(24):9907–9013.
24. Baker SN, Baker GA. Luminescent carbon nanodots: emergent nanolights. Angew Chem Int Ed. 2010; 49(38):6726–6744.
25. Li X, Wang H, Shimizu Y, Pyatenko A, Kawaguchi K, Koshizaki N. Preparation of carbon quantum dots with tunable photoluminescence by rapid laser passivation in ordinary organic solvents. Chem Commun. 2011; 47(3):932–934.
26. Hu SL, Niu KY, Sun J, Yang J, Zhaoa NQ, Du XW. One-step synthesis of fluorescent carbon nanoparticles by laser irradiation. J Mater Chem. 2009; 19(4):484–488.
27. Wang F, Pang S, Wang L, Li Q, Kreiter M, Liu CY. One-step synthesis of highly luminescent carbon dots in noncoordinating solvents. Chem Mater. 2010; 22(16):4528–4530.
28. Bourlinos AB, Stassinopoulos A, Anglos D, Zboril R, Karakassides M, Giannelis EP. Surface functionalized carbogenic quantum dots. Small. 2008; 4(4):455–458. [PubMed: 18350555]
29. Peng H, Travas-Sejdic J. Simple aqueous solution route to luminescent carbogenic dots from carbohydrates. Chem Mater. 2009; 21(23):5563–5565.
30. Bao L, Zhang ZL, Tian ZQ, Zhang L, Liu C, Lin Y, et al. Electrochemical tuning of luminescent carbon nanodots: from preparation to luminescence mechanism. Adv Mater. 2011; 23(48):5801–5806. [PubMed: 22144369]
31. Sun YP, Zhou B, Lin Y, Wang W, Shiral Fernando KA, Pathak P, et al. Quantum-sized carbon dots for bright and colorful photoluminescence. J Am Chem Soc. 2006; 128(24):7756–7757. [PubMed: 16771487]
32. Eda G, Lin YY, Mattevi C, Yamaguchi H, Chen HA, Chen IS, et al. Blue photoluminescence from chemically derived graphene oxide. Adv Mater. 2010; 22(4):505–509. [PubMed: 20217743]
33. Gokus T, Nair R, Bonetti A, Bohmler M, Lombardo A, Novoselov K, et al. Making graphene luminescent by oxygen plasma treatment. ACS Nano. 2009; 3(12):3963–3968. [PubMed: 19925014]

34. Stern ST, Zolnik BS, McLeland CB, Clogston J, Zheng J, McNeil SE. Induction of autophagy in porcine kidney cells by quantum dots: a common cellular response to nanomaterials? Toxicol Sci. 2008; 106(1):140–152. [PubMed: 18632727]
35. Park S, An J, Piner RD, Jung I, Yang D, Velamakanni A, et al. Aqueous suspension and characterization of chemically modified graphene sheets. Chem Mater. 2008; 20(21):6592–6594.
36. Hernandez Y, Nicolosi V, Lotya M, Bligue F, Sun Z, De S, et al. High-yield production of graphene by liquid-phase exfoliation of graphite. Nat Nanotechnol. 2008; 3(9):563–568. [PubMed: 18772919]
37. Ferrari AC, Robertson J. Interpretation of Raman spectra of disordered and amorphous carbon. Phys Rev B. 2000; 61(20):14095–14107.
38. Yuan D, Chen J, Hu X, Zeng J, Tan S, Liu Y. Large-scale synthesis of monodispersed carbon microflakes for electric double-layer capacitors. Int J Electrochem Sci. 2008; 3(11):1268–1276.
39. Lespade P, Al-Jishi R, Dresselhaus MS. Model for Raman scattering from incompletely graphitized carbons. Carbon. 1982; 20(5):427–431.
40. Lespade P, Marchard A, Couzi M, Cruege F. Caracterisation de materiaux carbones par microspectrometrie Raman. Carbon. 1984; 22(4–5):375–385.
41. Tuinstra F, Koenig JL. Raman spectrum of graphite. J Chem Phys. 1970; 53(3):1126–1131.
42. Dresselhaus MS, Jorio A, Souza Filho AG, Saito R. Defect characterization in graphene and carbon nanotubes using Raman spectroscopy. Philos Trans R Soc A. 2010; 368(1932):5355–5377.
43. Hoffmann R. Trimethylene and the addition of methylene to ethylene. J Am Chem Soc. 1968; 90(6):1475–1485.
44. Bourissou D, Guerret O, Gabbai FP, Bertrand G. Stable carbenes. Chem Rev. 2000; 100(1):39–91. [PubMed: 11749234]

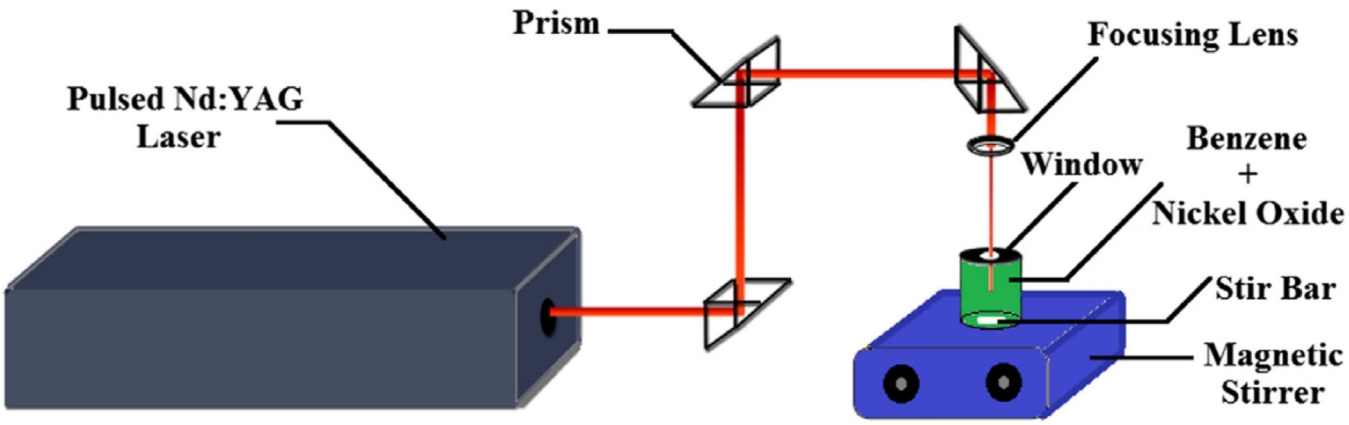

Fig. 1.
Detailed schematic of the experimental setup for the preparation of GQDs.

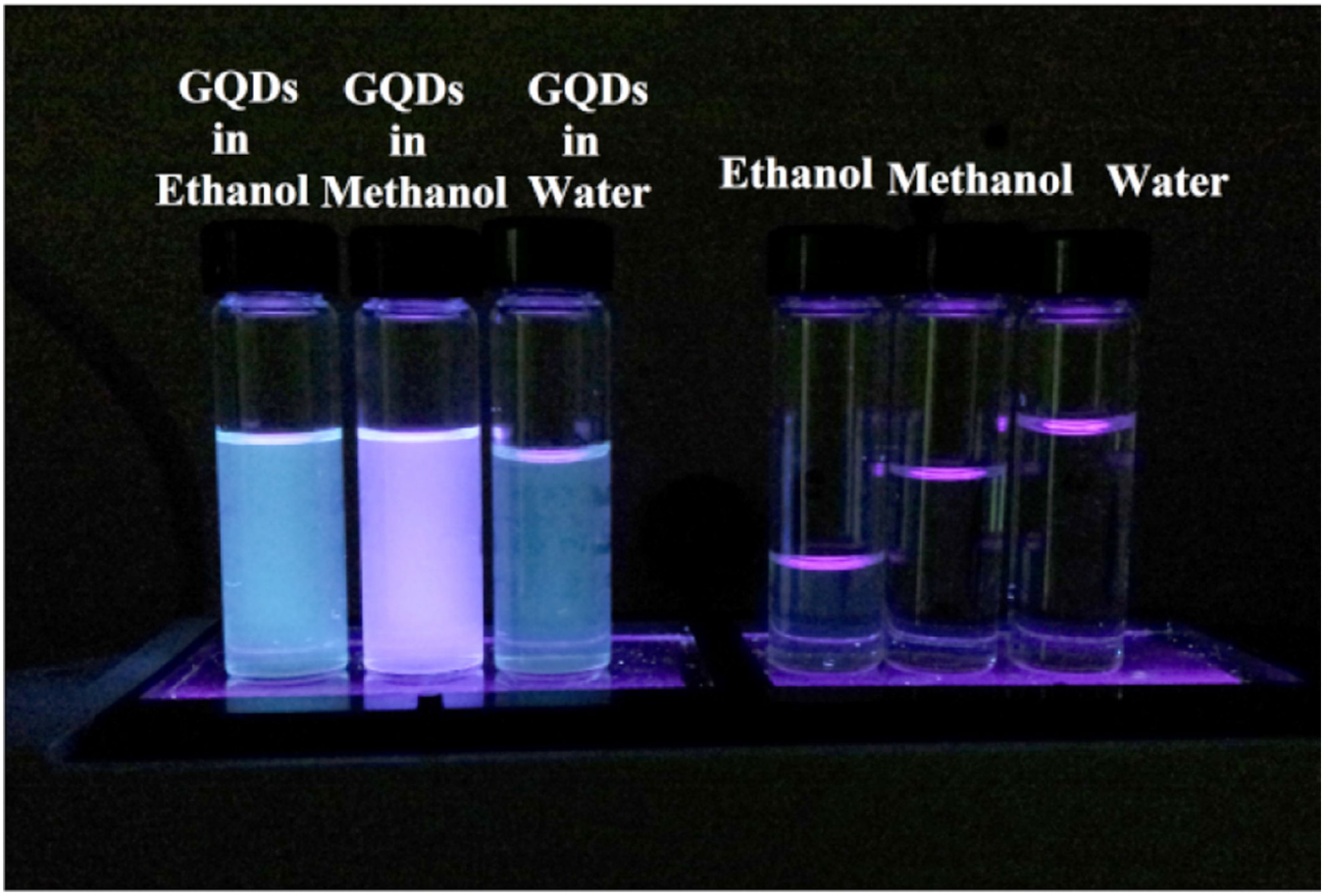

Fig. 2.
The as-grown nanoparticles show strong luminescence to the naked eye under UV light. The luminescence from the nanoparticles is distinguishable from that of the solvents.

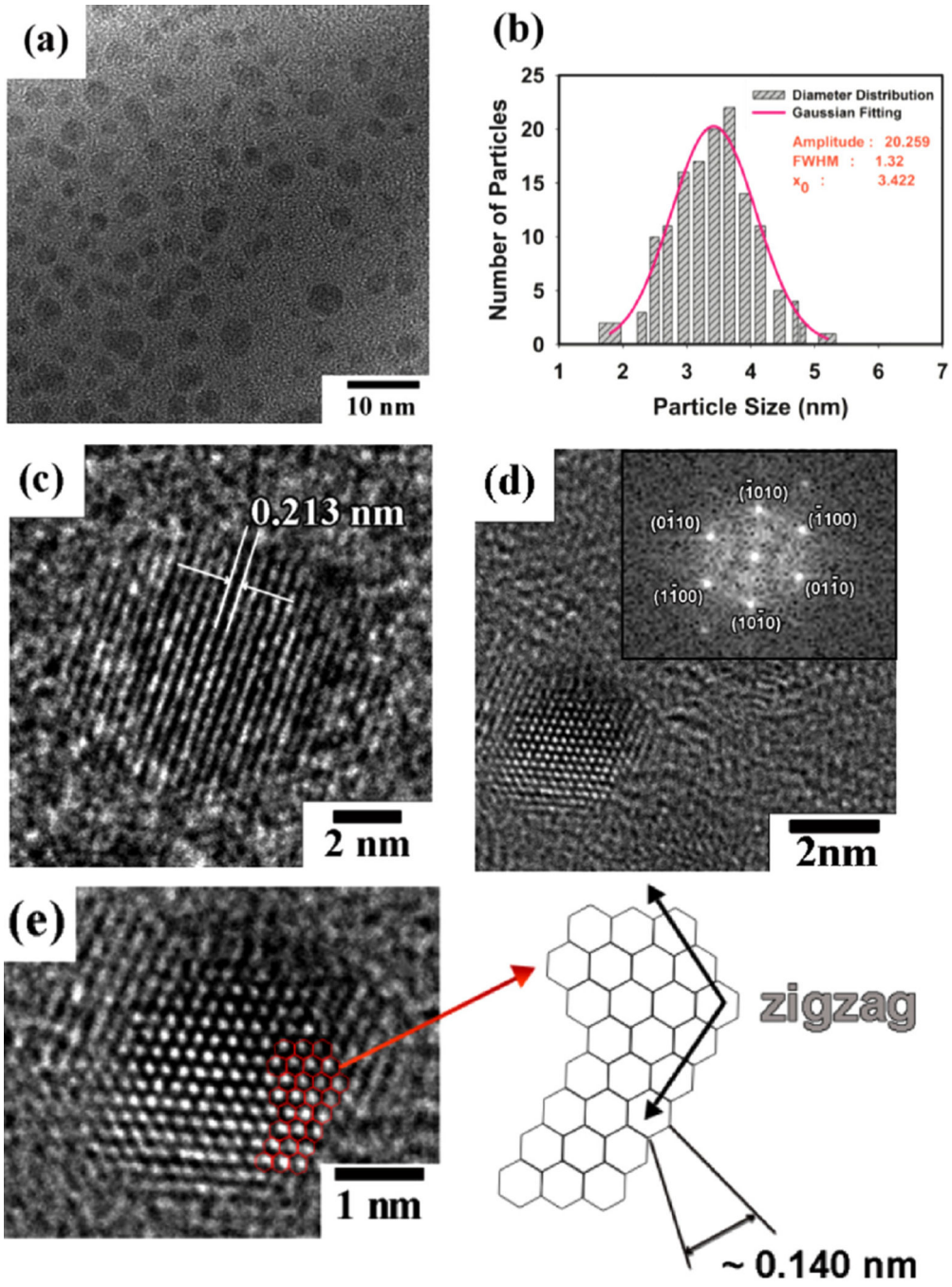

Fig. 3.

Characterization of the nanoparticles under HR-TEM showing: (a) the abundance and size range of the nanoparticles; (b) the statistical distribution of particle size peaking at 3.4 nm; (c) the measured lattice parameter of 0.213 nm corresponding to the (1100) in-plane lattice fringes of graphene; (d) the FFT analysis corresponding to the lattice fringes of graphene; and (e) the zigzag structure of the particles' edges consistent with graphene.

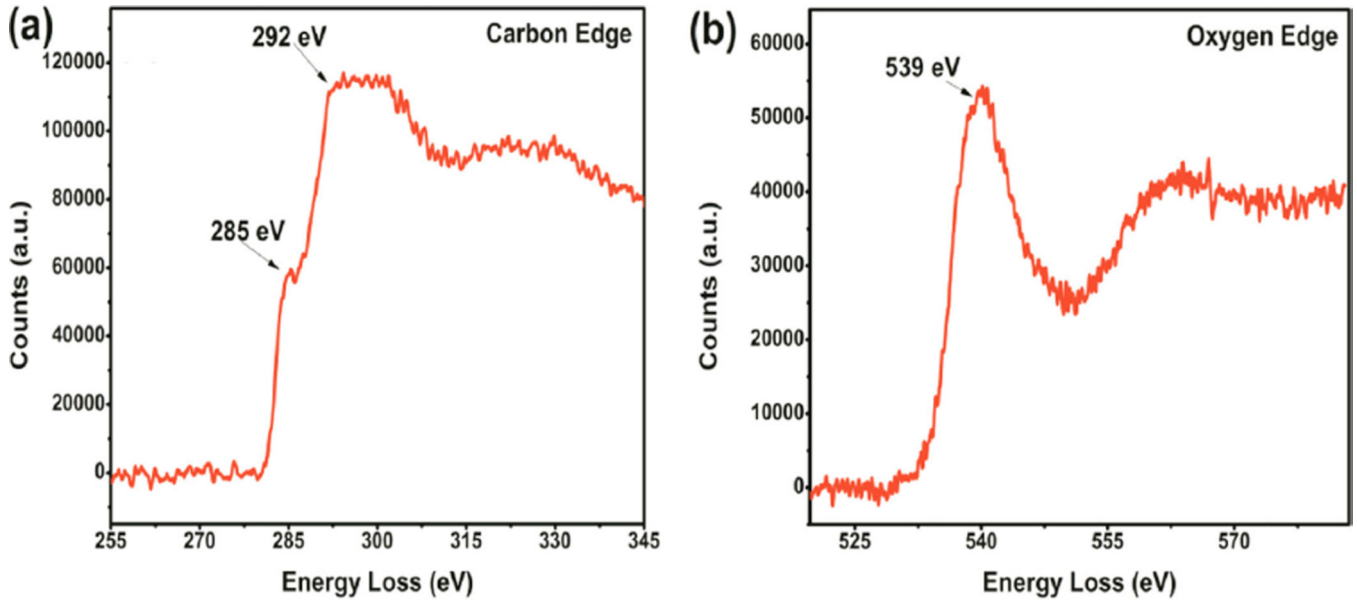

Fig. 4.

EELS spectra of the nanoparticles showing: (a) a prominent carbon edge around 292 eV, and (b) a weak oxygen edge around 539 eV.

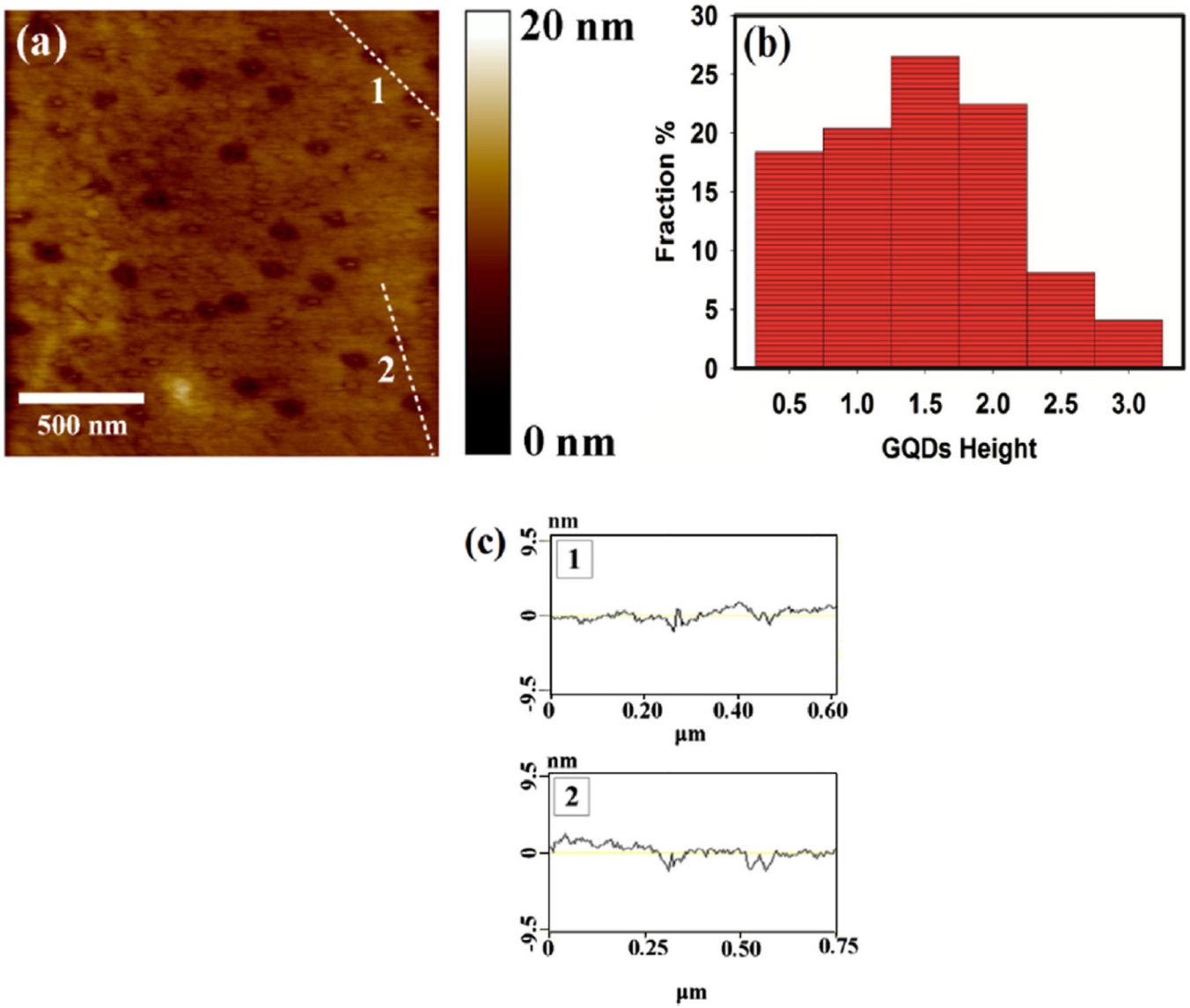

Fig. 5.

(a) AFM image of GQDs on mica substrate. (b) The histogram represents the topographic height distribution of GQDs based on the statistical analysis on the AFM image shown. (c) The height profile along the lines 1 and 2 shown in image (a).

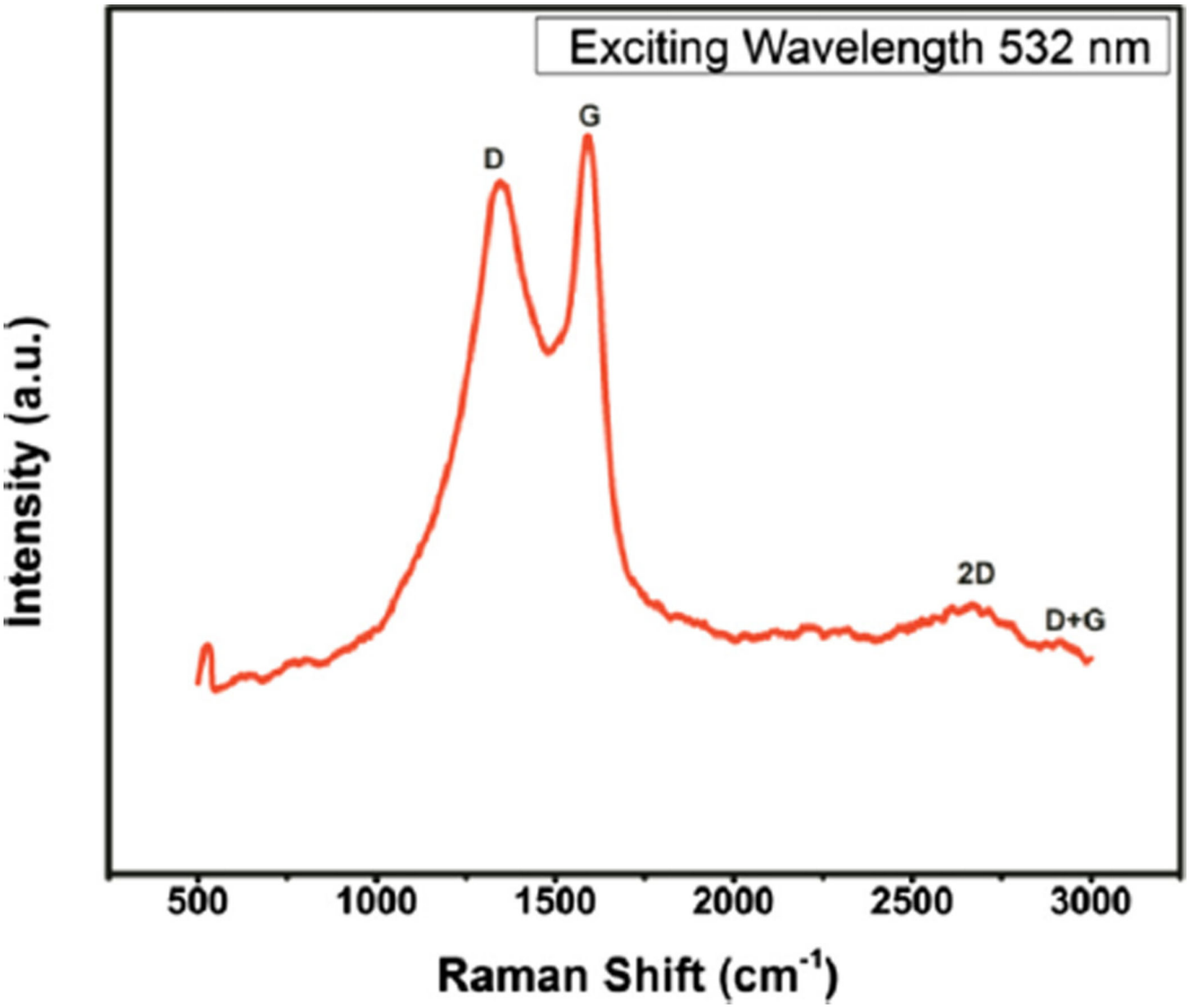

Fig. 6.

Raman spectrum of GQDs showing the D-band at 1352 cm^{-1}, G-band at 1594 cm^{-1}, and 2D band centered around 2670 cm^{-1}.

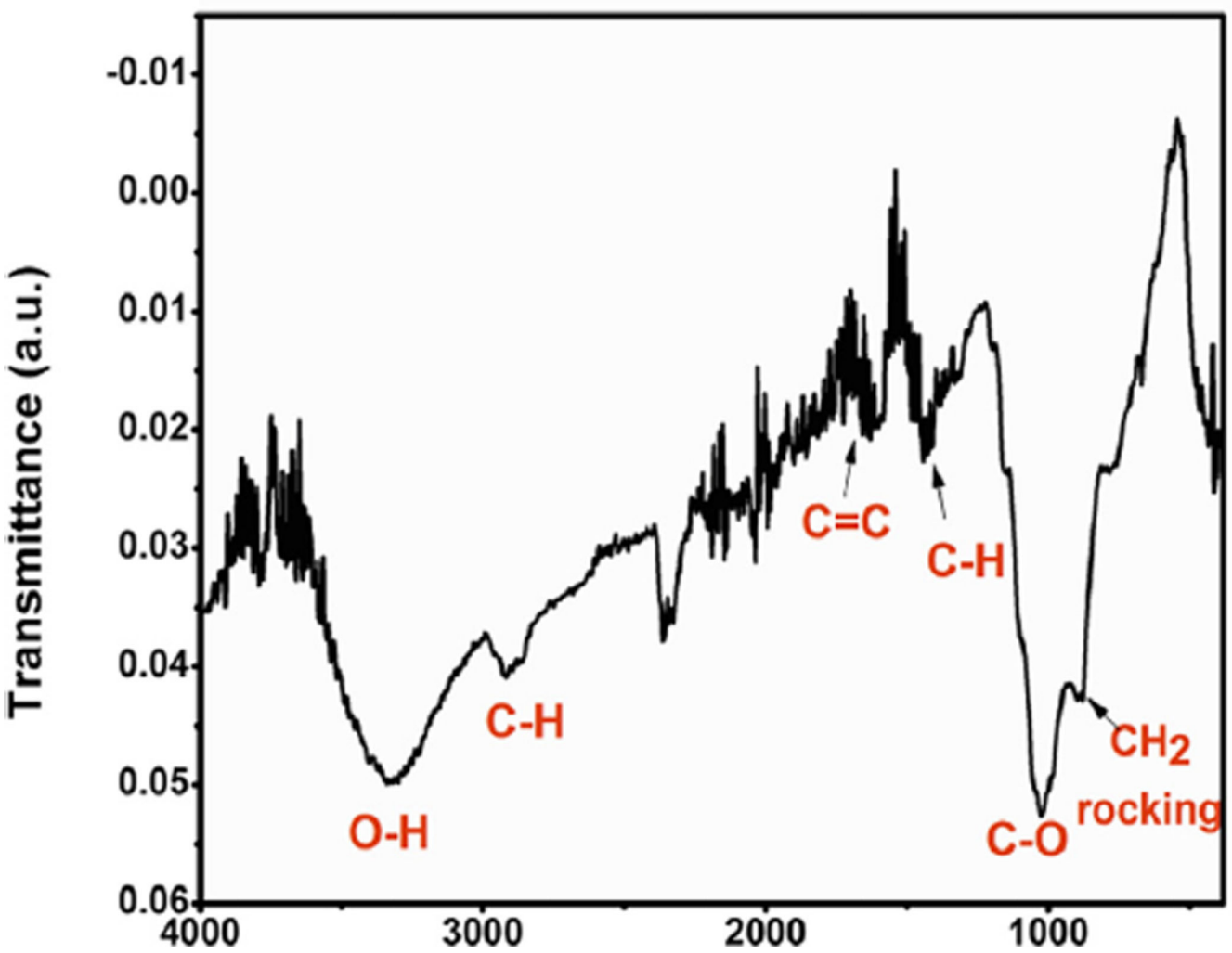

Fig. 7.

ATR FT-IR spectrum of GQDs on a silicon substrate. The absorption at 1620 cm $^{-1}$ is attributed to C=C bonds in aromatic carbon, the one at 1423 cm $^{-1}$ is assigned to −C−H bending, and the one at 2930 cm 1 is assigned C–H stretching. The spectrum also indicates the presence of C–O and hydroxyl groups on the surface of the GQDs.

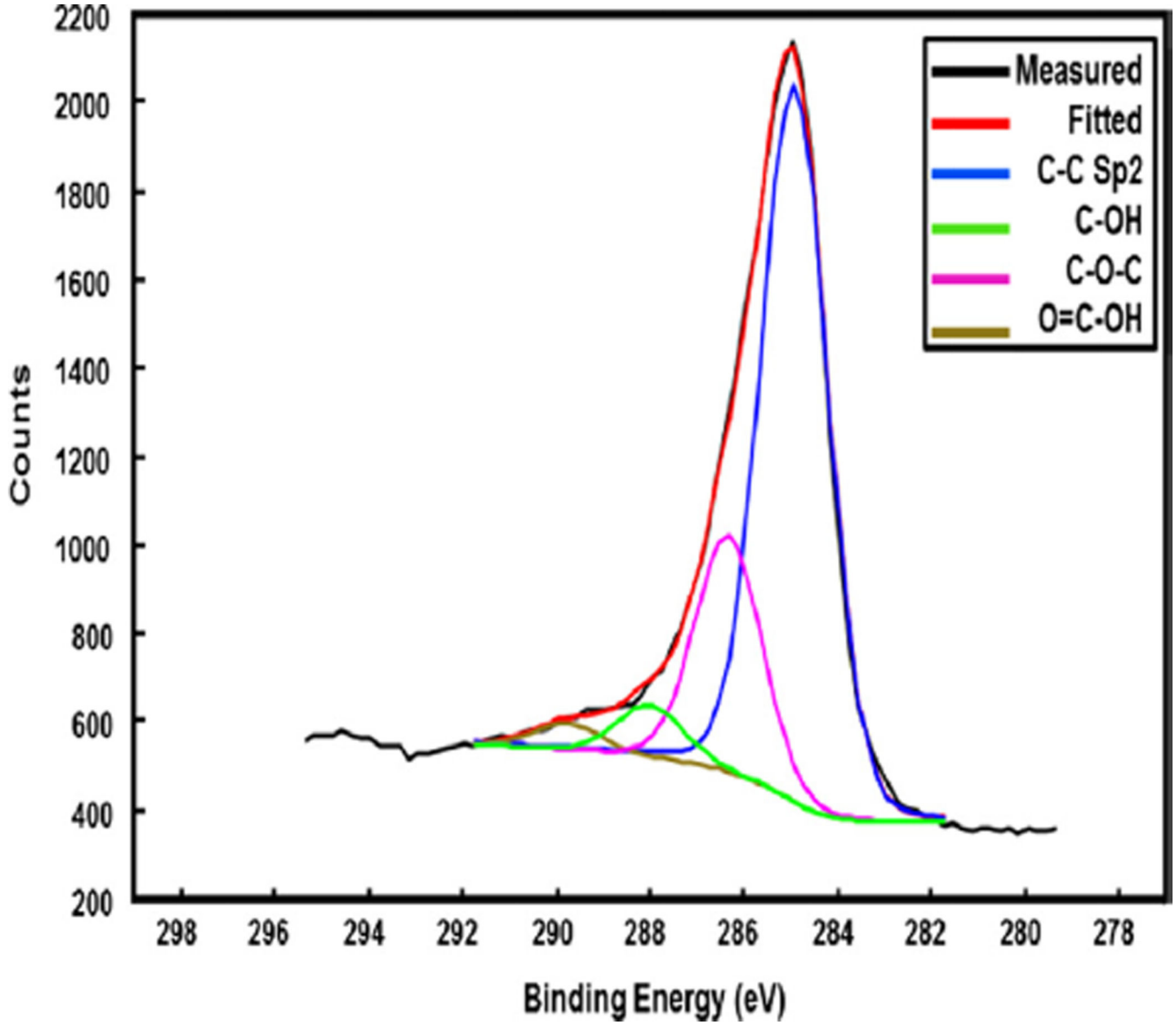

Fig. 8.

XPS spectrum of GQDs recorded at high resolution in the C1s region. The deconvolution of the spectrum shows the aromatic carbon C–C band at 284.9 eV and the presence of oxygen functionalities in the form of C–OH, C–O–C, and COOH corresponding to the frequencies at 286.3 eV, 287.85 eV, and 289.58 eV, respectively.

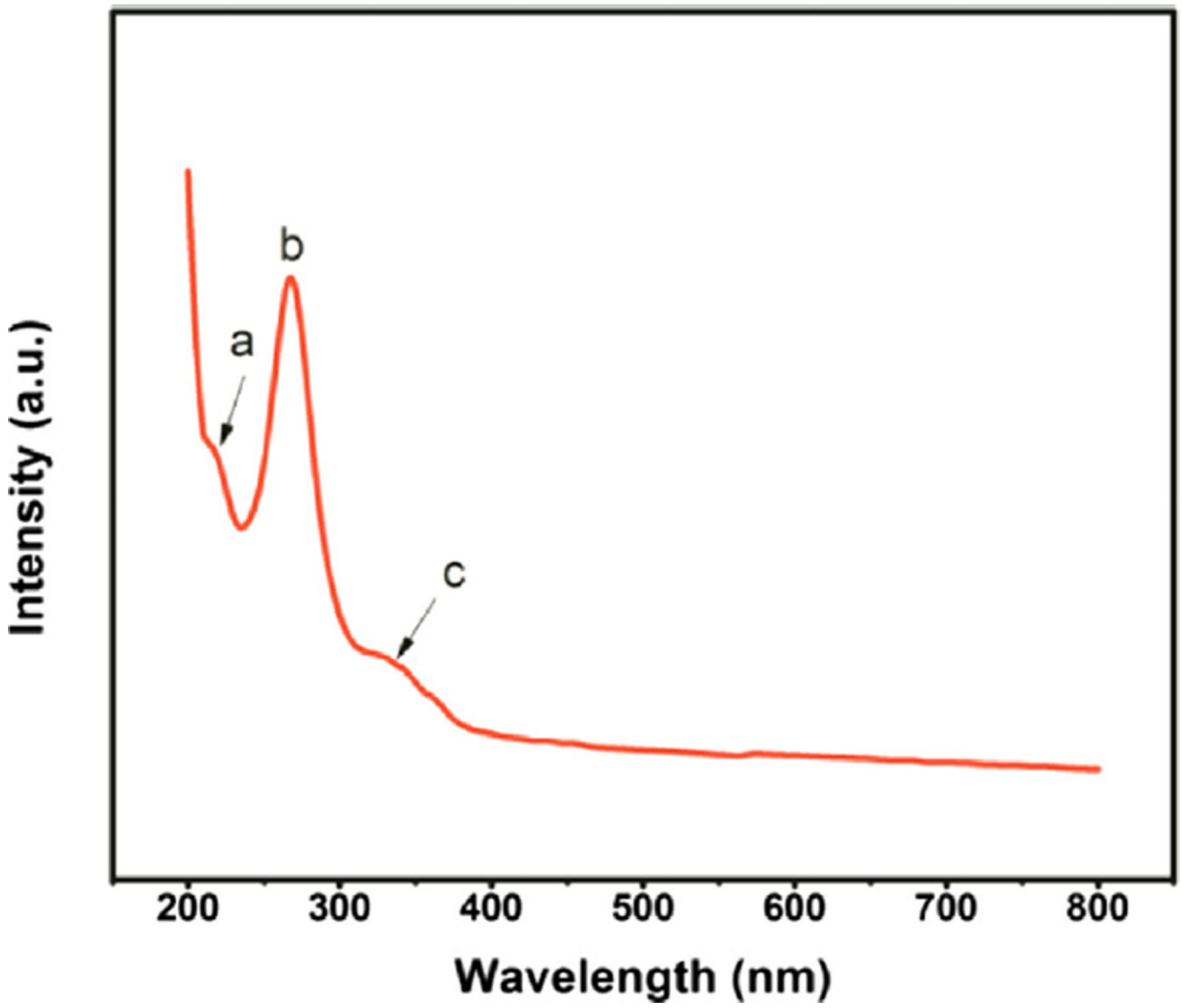

Fig. 9.

UV–Visible spectrum of the GQDs dissolved in water showing three absorption bands. The band at 217 nm corresponds to the π–π^* transition; the bands at 267 and 335 nm correspond to n–π^* transitions.

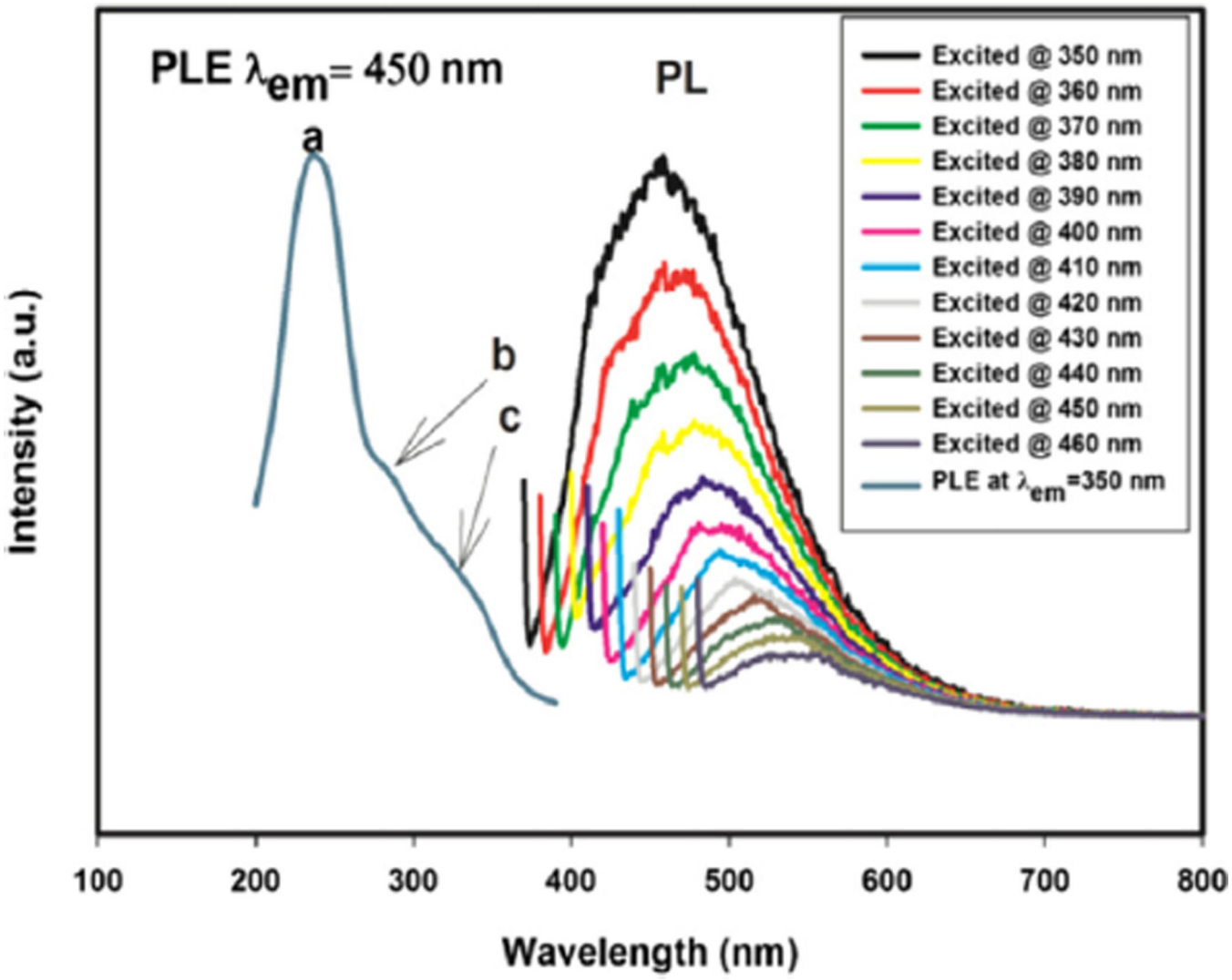

Fig. 10.

PL emission and PLE spectra of GQDs in water. GQDs emit visible light at different wavelengths depending on the wavelength of the excitation radiation. The PLE spectrum recorded at λ_{em} = 450 nm shows the presence of peak (a) centered around 237 nm, and shoulders (b) and (c) centered around 285 nm and 334 nm, respectively.

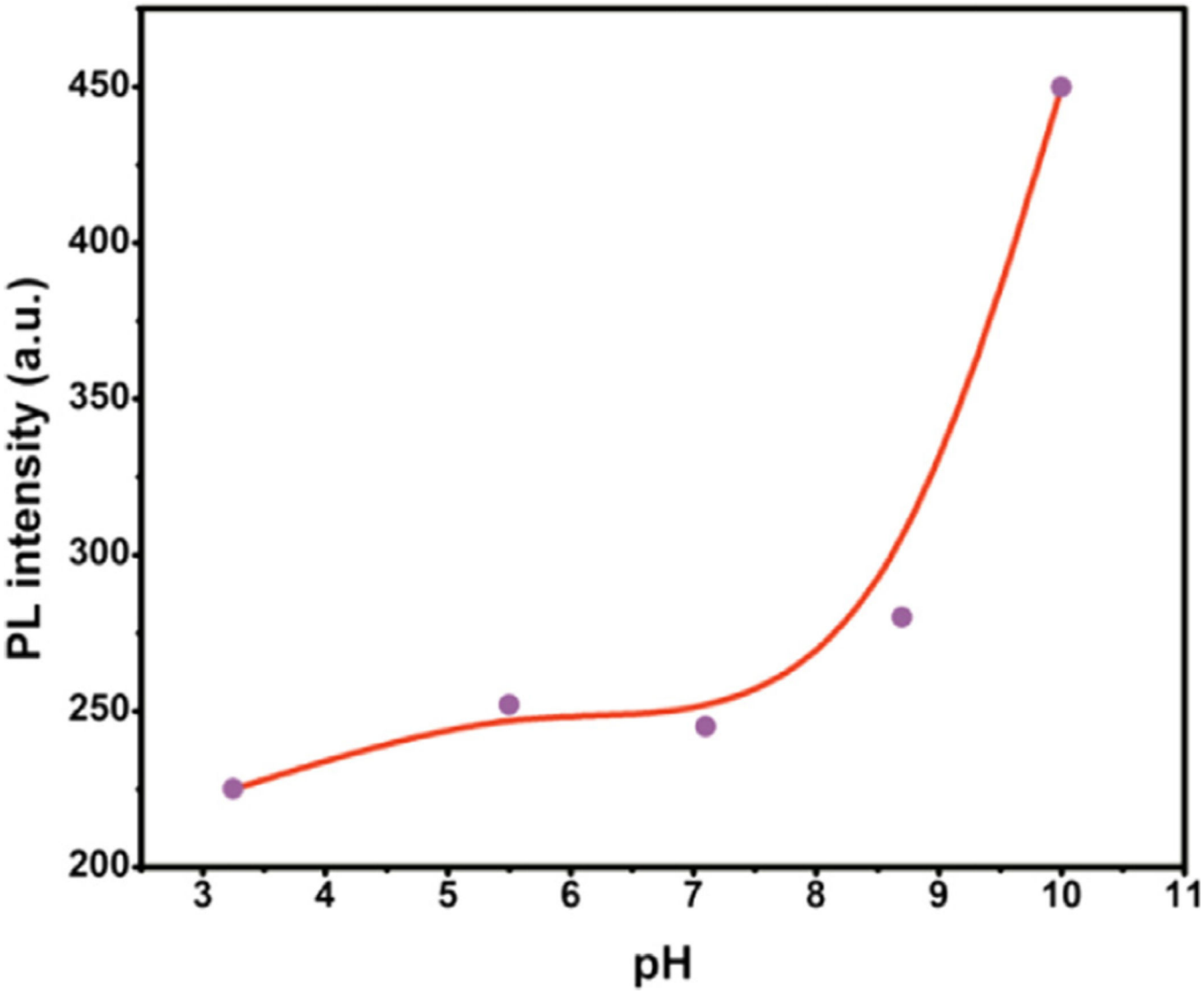

Fig. 11.

PL intensity as a function pH of the GQDs solution. The PL intensity of GQDs significantly increases in alkaline solution. The measurement of pH versus PL intensity was done by varying only the pH and under all same conditions.

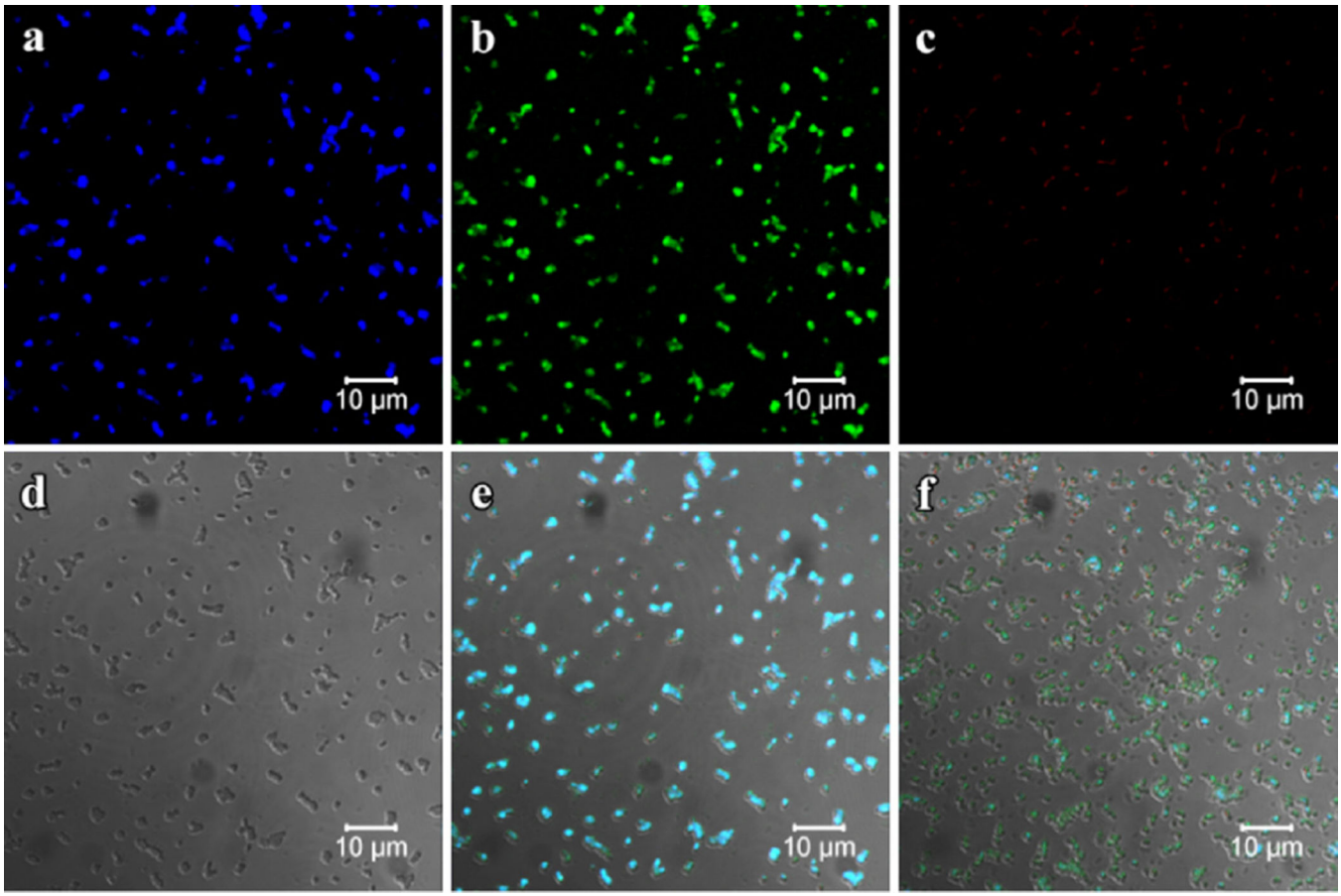

Fig. 12.

Confocal microscopy images of bacteria exposed to GQDs showing: (a) fluorescence in the 420–480 nm region; (b) fluorescence in the 520–555 nm region; (c) fluorescence in the 588–652 nm region; (d) bright field image of the bacteria; and (e) merge of images (a–d). The corresponding merge image of *Pseudomonas aeruginosa* bacteria without GQDs is shown in (f) to reveal the distinction between the bacteria self-fluorescence and the fluorescence arising from the GQDs linked to the bacteria.